Journal of Geosciences, 57 (2012), 173–188 DOI: 10.3190/jgeosci.123

Original paper

Late Triassic ^{40}Ar–^{39}Ar ages of the Baga-Gazryn Chuluu granites (Central Mongolia)

Katarzyna MACHOWIAK[1*], Wojciech STAWIKOWSKI[2], Stanisław ACHRAMOWICZ[3]

[1] *Institute of Civil Engineering, Poznań University of Technology, ul. Piotrowo 5, 61-138 Poznań, Poland; kamachow@amu.edu.pl*
[2] *Institute of Geology, Adam Mickiewicz University, ul. Maków Polnych 16, 61-606 Poznań, Poland*
[3] *Institute of Geological Sciences, Polish Academy of Sciences, ul. Podwale 75, 50-449 Wrocław, Poland*
[*] *Corresponding author*

New radiometric data have been obtained for two-mica granites from the Baga-Gazryn Chuluu Pluton in Central Mongolia, classified previously as A-type granites based on their geochemical characteristics and tectonic position. Three most common granite varieties were dated by ^{40}Ar–^{39}Ar method on separated biotite. The following ages were obtained: 201.0 ± 3.6 Ma (2σ) for the coarse-, 211.9 ± 4.0 Ma for the medium-, and 209.4 ± 3.2 Ma for the fine-grained granites. Such Late Triassic cooling ages agree well with the older assumptions on the time of emplacement of the Baga-Gazryn Chuluu Pluton, based on geological evidence and previous K–Ar dating. New geochronological data better constrain the age of granitic magmatism in post-collisional, extensional regime adjacent to the western part of the Mongol–Okhotsk suture zone in the Adaatsag area.

Keywords: Central Mongolia; Ar–Ar dating; Baga-Gazryn Chuluu; rare metal granite
Received: 19 December 2011; accepted: 29 September 2012; handling editor: M. Štemprok

1. Introduction

We present new cooling ages for biotite from the granites of the Baga-Gazryn Chuluu Pluton (BGC) in Central Mongolia, which are important for any discussion on the petrogenesis or relationships of this intrusion to other magmatic bodies located along the Mid-Mongolian Tectonic Zone (Tomurtogoo 1997). This first-scale tectonic lineament represents a suture after the closure of the last oceanic basin in the Mongolian part of the Altaids (Central Asian Orogenic Belt) – the Mongol–Okhotsk Ocean (e.g. Windley et al. 2007; Wilhem et al. 2012). Extensive Mesozoic magmatism in the northern part of Mongolia was directly linked with the closure of this oceanic domain (Donskaya et al. 2012).The BGC Pluton was emplaced into the zone of intense Phanerozoic continental accretion, connected with juvenile crust formation, typical of the Altaids (e.g. Jahn 2004; Jahn et al. 2009; Machowiak and Stawikowski 2012).

The first datings of the BGC granites and accompanying metasomatites have been made in early 1970's using the K–Ar technique (Kovalenko et al. 1971a). By the recent standards, the results were not satisfactory, as the ages spread over 65 Ma, with over 40 Ma ranges for individual rock varieties.

2. Geological setting and previous geochronology

The subject of the presented study is the granitic Baga-Gazryn Chuluu Pluton in Central Mongolia, with an outcrop area of *c.* 120 km^2 (Machowiak and Stawikowski 2012). The Pluton hosts numerous greisen bodies carrying Sn–W mineralization (Kovalenko et al. 1971a, b). The BGC granites were classified by the Soviet and Mongolian geologists (Kovalenko et al. 1971a, b) as belonging to the regional 'Sharakhadinskii' type of Li–F granites. By the latter authors, they were included into the group of the Early Mesozoic intrusions (*c.* 230–180 Ma) with the maximum of magmatic activity at *c.* 210 Ma.

The BGC Pluton has been chosen for the study due to its specific tectonic position close to the fault systems of broadly defined Mid-Mongolian Tectonic Line (Tomurtogoo 1997) as well as a peculiar geochemical signature. The BGC granites display alkaline characteristics, and are enriched in REE and other elements of potential economic value (Kovalenko et al. 1971a; Machowiak and Stawikowski 2012). In Europe, granites having a similar geochemical signature are rare. The investigated plutonic body is situated *c.* 30 km SW of the Adaatsag ophiolite (Tomurtogoo et al. 2005; Bussien et al. 2011), a relic of

oceanic lithosphere preserved after the Mongol–Okhotsk Ocean closure (Fig. 1).

In the tectonic division of Mongolia (Badarch et al. 2002), the studied igneous body belongs to the Middle Gobi Belt (MGB), a large volcano–plutonic unit of Permian–Mesozoic age. It is located close to the NW boundary of the MGB with the Adaatsag Terrane, interpreted as a former accretionary wedge (Badarch et al. 2002) transformed into a suture zone (Bussien et al. 2011).

According to previous interpretations based on the K–Ar dating and regional geological context (Kovalenko et al. 1971a, b), the BGC granites intruded into Permian volcano–sedimentary rocks of the MGB in the Early Mesozoic times (Tomurtogoo et al. 1998–2002; Fig. 2). The Pluton emplacement caused a relatively narrow contact aureole of hornfelses, suggesting a shallow level of intrusion (Machowiak and Stawikowski 2012).

Thirteen rock samples from the BGC Pluton have been previously dated on whole-rock samples as well as biotite and K-feldspar concentrates by K–Ar technique (Kovalenko et al. 1971a). The measured ages of all these rocks were strongly scattered between 246 and 171 Ma. Four coarse-grained granites, called 'alaskites of the main intrusive phase', yielded ages of 235–192 Ma, three fine-grained granites – 'alaskites of the late intrusive phase' – gave 236–192 Ma, 4 greisens 246–200 Ma and two microclinites 236–171 Ma.

Small (several meters in size) outcrops of trachyandesites are scattered near the contact with the BGC Pluton (Fig. 2) and bigger, up to several tens of meters long bodies situated *c.* 10 km to NE of the BGC Pluton. In the literature (Kovalenko et al. 1971a) and on the geological map of the studied area (Tomurtogoo et al. 1998–2002), the trachyandesites were described as plagioclase porphyries and assigned to Jurassic or Permian, whereas the age of the BGC Pluton was considered to be Late Triassic/Early Jurassic or Middle Jurassic. The trachyandesites are surrounded by the rocks of Permian volcano-sedimentary sequence (Machowiak and Stawikowski 2012).

3. Methods

3.1. Electron-microprobe analysis (EPMA)

The electron-microprobe studies on mineral chemistry from the granites and greisens of the BGC Pluton have been conducted on *c.* 15 polished thin sections at the Institute of Mineralogy, Leibnitz University in Hannover and the Joint-Institute Analytical Complex for Minerals and Synthetic Substances, Warsaw University, using the Cameca SX-100 apparatuses. All the analyses have been performed using the WDS (wavelength dispersion) technique, with 15 kV accelerating voltage, 10 and 20 s counting times and a beam current of 20 or 10 μA. Mineral standards as well as PAP and ZAF correcting procedures have been applied (Reed 1993).

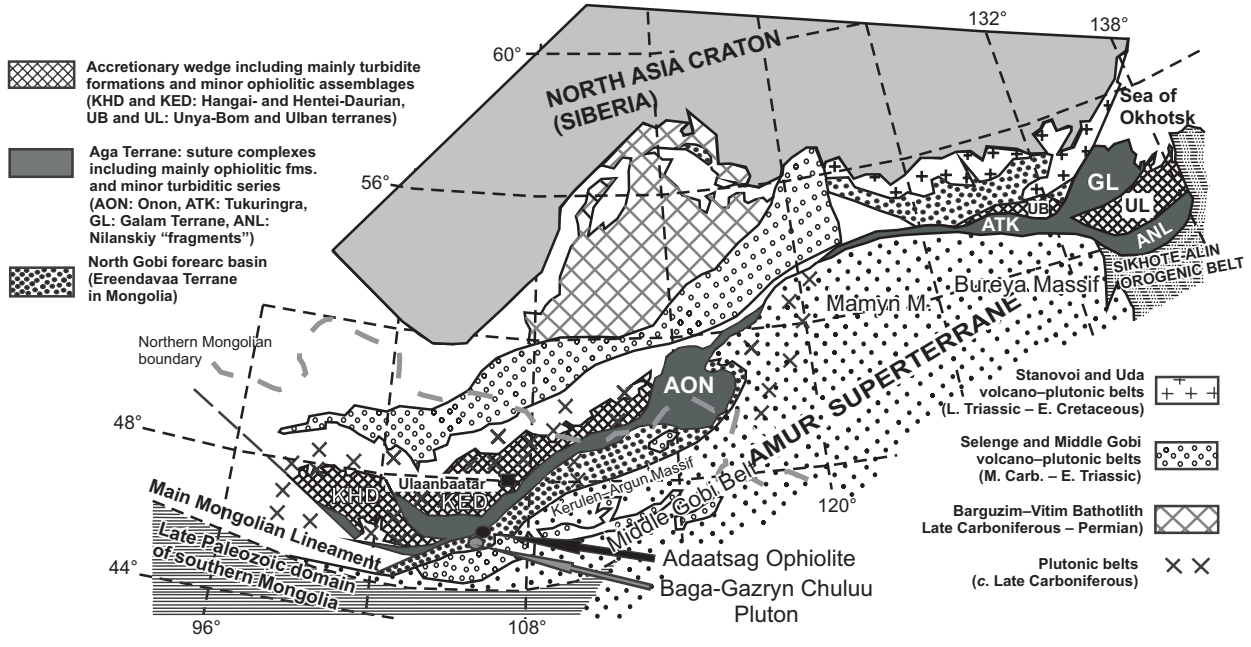

Fig. 1 Position of Baga-Gazryn Chuluu Pluton at the tectonic sketch map of the Mongol–Okhotsk Belt and the framing units (after Bussien et al. 2011, modified).

3.2. Whole-rock geochemistry

Almost seventy bulk chemical analyses of the rocks from the Baga-Gazryn Pluton area have been carried out. Apart from granites, also trachyandesites and greisens have been examined. The samples destined for geochemical investigations were hand-crushed and powdered in a tungsten carbide mill at the Institute of Geology, Adam Mickiewicz University in Poznań. All the bulk rock chemical analyses were conducted by Activation Laboratories Ltd. in Ontario, Canada. The results were obtained using X-ray fluorescence (XRF), neutron activation analysis (INAA) and inductively-coupled plasma – atomic emission spectrometry (ICP-AES). The analytical procedures and the information about the applied standards in the 4Litho package are available at the ACTLABS website (*http://www.actlabs.com/files/Euro_2011.pdf)*. In order to test the degree of possible contamination of the samples with W and Co during milling, the contents of these elements in a pure SiO_2 have been measured. The results of the geochemical analyses have been corrected taking into account the obtained level of contamination.

3.3. ^{40}Ar–^{39}Ar

Three fresh samples of granite were selected for ^{40}Ar–^{39}Ar analyses. The biotite fraction has been separated using heavy liquids ($Na_6(H_2W_{12}O_{40})H_2O$, density of 3.0 g/cm^3). Subsequently, the biotite flakes were hand-picked under the microscope. Such biotite concentrates have been sent to Activation Laboratories Ltd., in Canada. The samples wrapped in Al foil were loaded in evacuated and sealed quartz vial with K and Ca salts and packets of LP-6 biotite interspersed with the samples to be used as a flux monitor. The samples were irradiated in the nuclear reactor for 48 hours. The flux monitors were placed between every two samples, thereby allowing precise determination of the flux gradients within the tube. After the flux monitors were run, the J-values were calculated for each

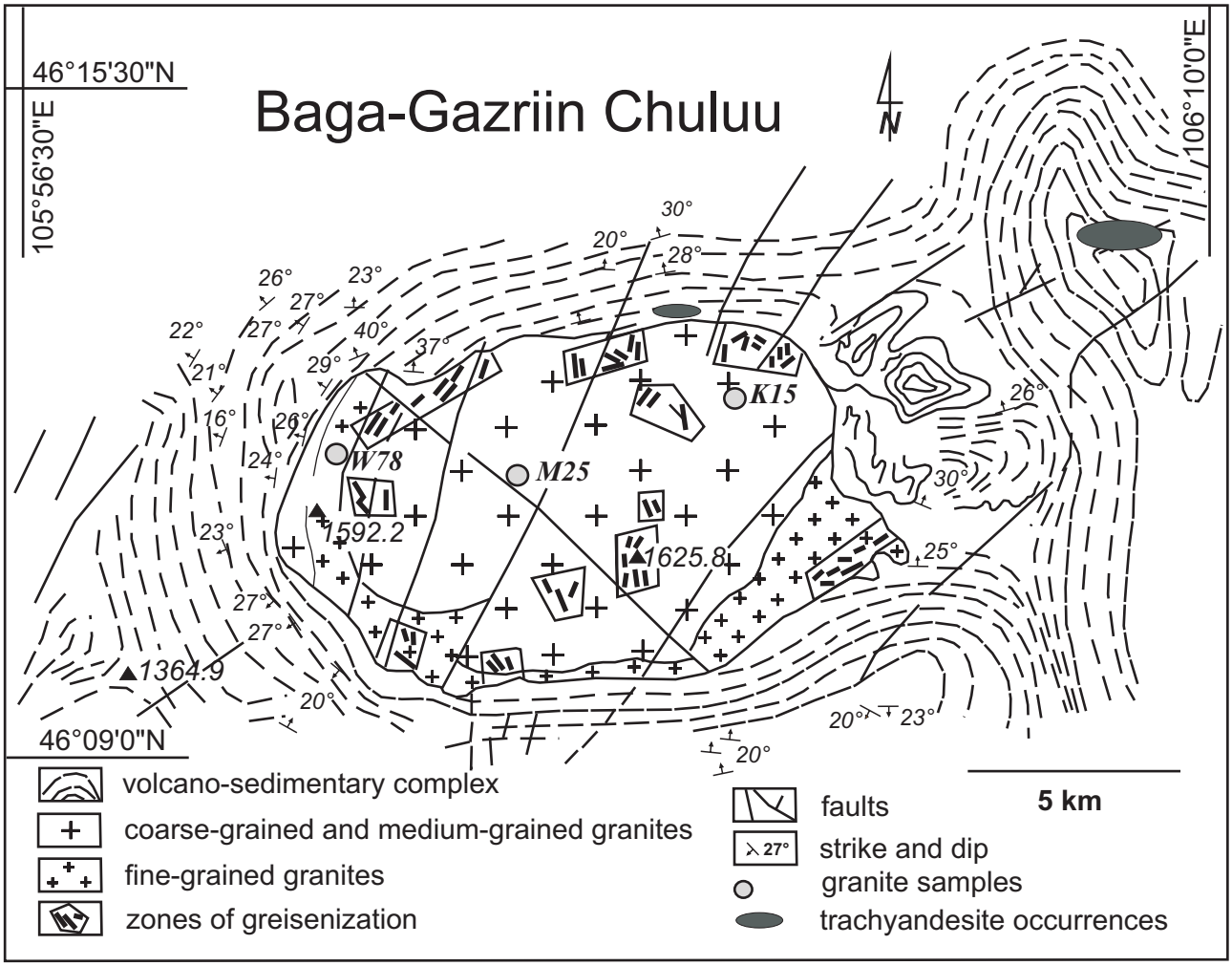

Fig. 2 Geological sketch of the Baga-Gazryn Chuluu Pluton (after Kovalenko et al. 1971a, Machowiak and Stawikowski 2012, modified).

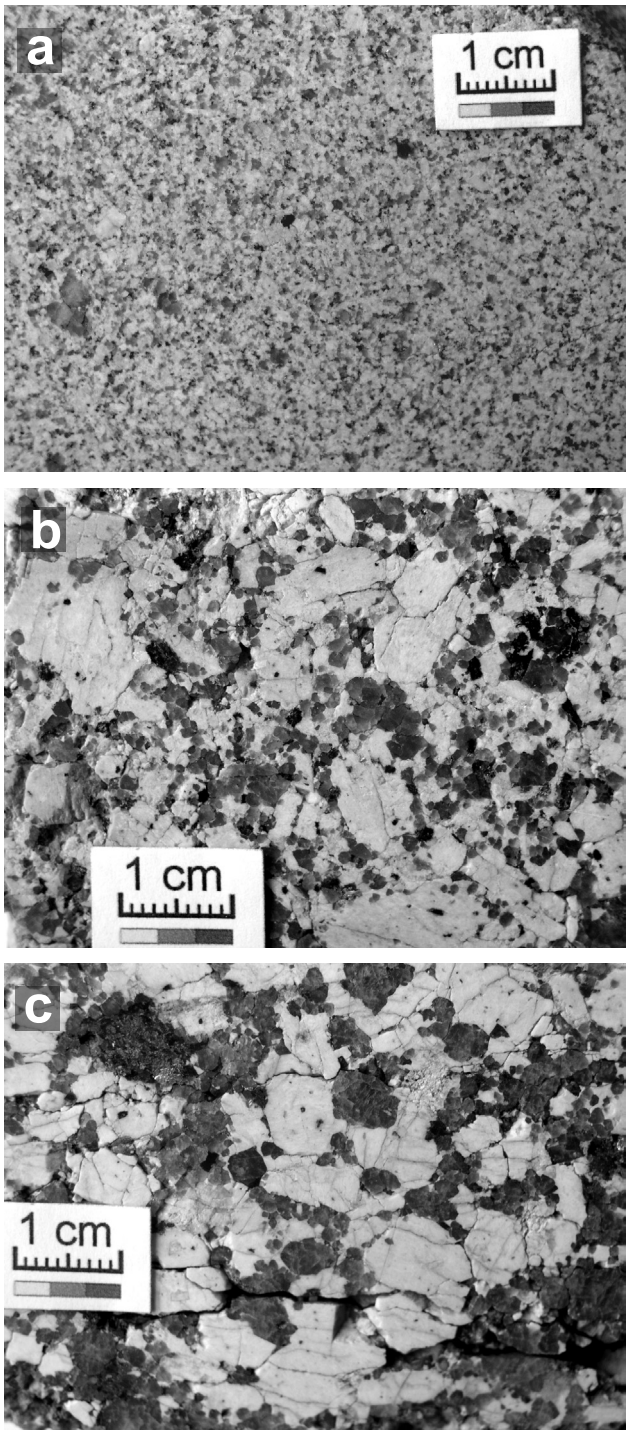

Fig. 3 Macrophotographs of dated samples from the Baga-Gazryn Chuluu Pluton: **a** – fine-grained equigranular granite W78; **b** – medium-grained porphyritic granite K15, **c** – coarse-grained porphyritic granite M25.

sample, using the measured flux gradient. The LP-6 biotite has an assumed age of 128.1 Ma. The neutron gradient did not exceed 0.5 % on sample size. The Ar isotope composition was measured in a Micromass 5400 static mass spectrometer. The 1200 ºC blank of ^{40}Ar did not exceed $n\times10^{-10}$ cm^3 STP (Standard Temperature and Pressure). The errors for biotite Ar–Ar ages are quoted at 2 sigma level.

4. Rock description and chemical composition of minerals

4.1. Baga-Gazryn Chuluu granites

The Baga-Gazryn Chuluu granites are divided into three textural varieties (Machowiak and Stawikowski 2012):

- fine-grained equigranular granites (Fig. 3a) and fine-grained porphyritic granites, occurring mostly in the marginal zone (Fig. 2);
- medium-grained porphyritic granites (Fig. 3b) with occurrences scattered all over the Pluton;
- coarse-grained equigranular, locally porphyritic granites (Fig. 3c) – mainly in the inner part of the Pluton (Fig. 2).

However, field observations have revealed strong textural heterogeneity of the BGC Pluton. The individual varieties pass into each other over small distances, which makes the precise distribution of the three facies unmapable. Therefore, the presented sketch of the Pluton (Fig. 2) indicates the domination of the granite varieties in given parts of the intrusion, not their exclusive occurrences. The contacts between them, even though frequently sharp, are often uneven and gradual, corresponding to plastic behavior of the solidifying magmas. The BGC granites do not contain any enclaves (Machowiak and Stawikowski 2012).

The granites of the BGC Pluton display monotonous modal composition with K-feldspar (35 to 50 vol. % in the rock; $Or_{90–99}Ab_{10–1}$), quartz (25 to 40 vol. %), plagioclase (3 to 10 vol. %; $An_{0–10}$) (Fig. 4a), biotite (max. 5 vol. %), $(K_{1.03–0.96}Na_{0.04–0.0})(Al_{0.84–0.54}Ti_{0.18–0.03}Fe_{1.78–1.62}Mg_{0.07–0.06})(Si_{2.92–2.84}Al_{1.16–1.08})O_{10}(OH)_2$ and muscovite (max. 3 vol. %), $(K_{0.91–0.89}Na_{0.01})(Al_{1.80–1.77}Fe_{0.16–0.14}Mg_{0.05–0.04})(Si_{3.30–3.29}Al_{0.70–0.69})O_{10}(OH)_2$ as the main rock-forming minerals. The samples influenced by greisenization contain also topaz, fluorite, REE minerals (mainly monazite) and lithium micas – zinnwaldite (Fig. 4b) and lepidolite.

In all porphyritic varieties of the BGC granites, phenocrysts are mainly idiomorphic or hypidiomorphic, perthitic K-feldspars. The potassium feldspars form also smaller hypidio- to xenomorphic grains in the groundmass. Quartz is xenomorphic and usually displays undulose extinction. The plagioclases are mostly unzoned. They occur subordinately, in some samples sparsely. Sporadically, myrmekites are observed. Biotites are usually hypidiomorphic, while less frequently

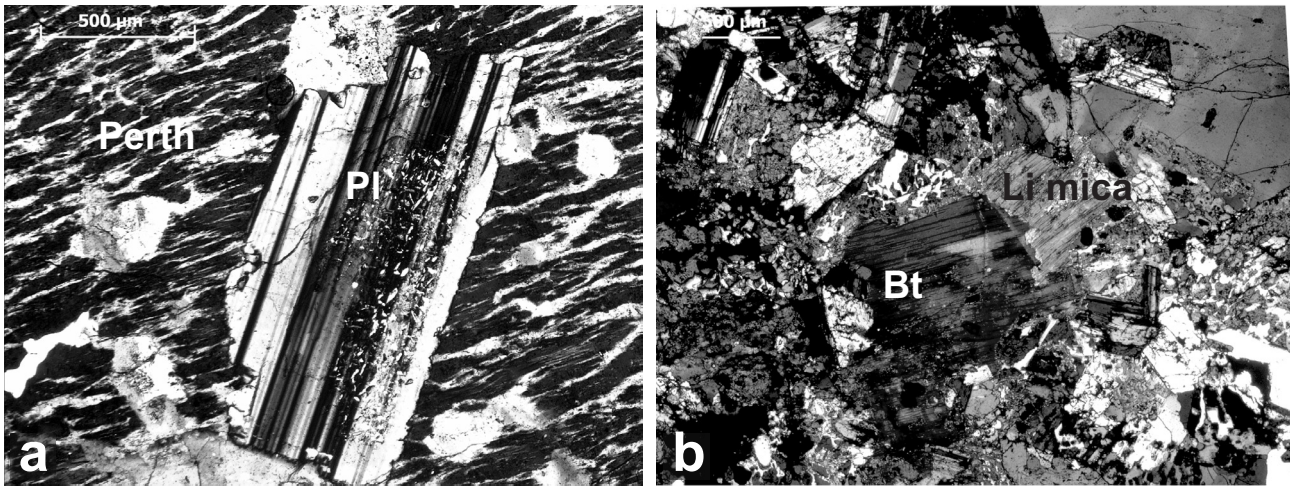

Fig. 4a – Photomicrographs (crossed nicols) of typical medium-grained granite (sample K25) from the Baga-Gazryn Chuluu Pluton: **a** – plagioclase inclusion in perthitic K-feldspar; **b** – biotite accompanied by Li-mica (zinnwaldite).

observed white micas (muscovite or lepidolite) display xenomorphic shapes. The white micas occur mainly in greisenized samples, either in the interstices or replacing K-feldspar and biotite. In part of the samples, the biotite is accompanied by probably secondary (seemingly postmagmatic) muscovite; elsewhere it is associated with lepidolite. Systematic positions of the micas are presented in the mgli–feal diagram (Tischendorf et al. 2004, Fig. 5).

The electron-microprobe analyses of micas (Tab. 1) have shown that biotites are characterized by very low MgO (0.13–1.1 wt. %, usually 0.68 wt. %) and very high FeO (20–28 wt. %, typically 24–26 wt. %). As for the micas, fairly high is the content of MnO (0.2–1.5 wt. %, usually 0.5–0.7 wt. %) and Al_2O_3 (17–20 wt. %). Accordingly, the Al concentrations in the octahedral sites are very high (0.5–1.2 *apfu*, most frequently 0.6–0.8 Al^{IV} *apfu*).

The muscovites display high SiO_2 (47–49 wt. %), increased Al_2O_3 (24–30 wt. %) and K_2O (10.2–11.0 wt. %) contents, low FeO (2.3–2.7 wt. %) and elevated (compared to the remaining micas) Al concentrations in the octahedral sites (Al^{IV} = 1.7–1.8 *apfu*). The sums of octahedral cations are close to 2.0 *apfu*, and the rest is assumed to be Li^{2+}, which could not be determined by the EPMA. Typical potassium micas from the granites studied are solid solutions of muscovite (0.72–0.76 mol. %), Fe-celadonite (0.15–0.17 mol. %), Mg-celadonite (0.055–0.060 mol. %) and polylithionite (0.01–0.06 mol. %).

The presence of zinnwaldite in the studied rocks is indicated by high ('muscovitic') interference colours, conspicuous greenish- passing to grey- passing to brown pleochroism, and systematically observed deficiency in cations of the biotite octahedral sites, ranging between 0.37 and 0.55 *apfu*. It was assumed that such a portion in the structure of all the studied biotites (trioctahedral mica) is occupied by Li. This assumption extends the isomorphic series of biotite (White et al. 2007; Tajčmanová et al. 2009) with the lithium members: polylithionite [$KLi_2AlSi_4O_{10}F_2$] and masutomilite [$KLiAlMn^{2+}(AlSi_3)O_{10}F_2$], which contains Li and Mn in one member (Rieder et al. 1998).

Zinnwaldite is defined as a series of trioctahedral potassium Fe–Li–Al micas (Tab. 1, Fig. 5) with a composition transitional between siderophyllite and polylithionite (Rieder et al. 1998). The presented results document zinnwaldite as a solid solution in the annite–polylithionite–muscovite–masutomilite series. Its composition changes over a rather narrow range: annite 0.115–0.118 mol. %, polylithionite 0.366–0.375 mol. %, muscovite 0.475–0.480 mol. % and masutomilite 0.035–0.042, while the Ti-biotite and siderophyllite proportions are close to zero.

Lepidolite, when referring to the isomorphic series of potassium Fe–Li–Al (Mn,Mg,Ti) micas as well as in comparison to the muscovite composition, does not include Fe-celadonite, Mg-celadonite and siderophyllite members (Tab. 1, Fig. 5). All the Fe^{2+} is represented by annite. The lepidolite from the BGC granites is a solid solution between muscovite (0.47–0.57 mol. %), masutomilite (0–0.005 mol. %), polylithionite (0.37–0.48 mol. %) and annite (0.05–0.09 mol. %).

The most common accessories are zircon and monazite, found as very small grains (<50 µm) enclosed mainly by biotite. Apatite and opaque phases have not been observed. Lithium micas and muscovites are usually devoid of the two. Depending on the degree of greisenization, variable contents of topaz, fluorite and mica aggregates (usually biotite–zinnwaldite) are observed. The BGC granites display no clear evidence for hydrothermal alteration.

Tab. 1 Composition of selected micas and molar proportions of end members of Fe–Li–Al–(Mg–Mn–Ti) potassium mica isomorphic series in granites and greisens of the Baga-Gazryn Chuluu Pluton

mica	biotite					biotite/zinnwaldite		zinnwaldite	lepidolite	muscovite			
rock	greisen		granite			granite				greisen		granite	
sample	MW58.1	MW58.2	$K25.1_{core}$	$K25.1_{rim}$	$M25.4_{core}$	$M25.4_{rim}$	M1.4	W78.1	M30B.7	M25.5	W1.10	M30B.5	M30B.6
SiO_2	35.43	35.7	35.58	36.58	35.66	47.03	47.69	38.72	47.24	50.2	47.71	48.51	48.87
TiO_2	1.99	2.70	2.95	2.66	0.55	0.20	0.02	1.00	0.11	0.04	0.06	0.04	0.31
Al_2O_3	18.81	18.16	17.82	18.78	19.97	27.02	27.79	20.16	29.57	26.44	30.25	31.21	30.95
FeO	26.28	26.82	26.57	25.79	23.64	7.74	7.91	20.34	4.85	5.18	2.33	2.44	2.77
MnO	0.91	0.91	0.54	0.48	0.59	0.26	0.51	0.72	0.01	0.00	0.3	0.05	0.01
MgO	0.60	0.48	0.50	0.51	0.57	0.56	0.39	0.31	0.42	0.84	0.00	0.41	0.48
CaO	0.04	0.01	0.04	0.02	0.04	0.05	0.02	0.07	0.37	0.23	0.06	0.14	0.01
Na_2O	0.19	0.24	0.17	0.16	0.00	0.10	0.00	0.28	0.19	0.10	0.03	0.08	0.07
K_2O	9.98	9.98	10.11	10.20	9.36	10.65	9.90	9.00	8.52	8.4	10.7	10.33	10.59
H_2O	3.74	3.76	3.74	3.81	3.67	4.27	4.41	3.78	4.31	4.32	4.32	4.41	4.45
Σ	97.96	98.76	98.01	98.98	94.04	97.88	98.66	94.39	95.59	95.76	95.75	97.61	98.51
Si	2.838	2.844	2.854	2.879	2.915	3.287	3.274	3.071	3.290	3.484	3.319	3.298	3.302
Al^{IV}	1.162	1.156	1.146	1.121	1.085	0.713	0.726	0.929	0.710	0.516	0.681	0.702	0.698
ΣT	4.000	4.000	4.000	4.000	4.000	4.000	4.000	4.00	4.000	4.000	4.000	4.000	4.000
Al^{VI}	0.614	0.549	0.539	0.621	0.840	1.513	1.523	0.956	1.718	1.647	1.800	1.800	1.767
Ti	0.120	0.162	0.178	0.157	0.034	0.011	0.003	0.060	0.006	0.000	0.003	0.000	0.016
Fe^{2+}	1.761	1.787	1.782	1.698	1.616	0.452	0.455	1.349	0.280	0.301	0.136	0.139	0.157
Mn	0.062	0.061	0.037	0.032	0.041	0.015	0.030	0.048	0.001	0.000	0.018	0.003	0.001
Mg	0.072	0.057	0.060	0.060	0.069	0.058	0.040	0.037	0.044	0.087	0.000	0.042	0.048
ΣY	2.629	2.616	2.596	2.568	2.600	2.049	2.051	2.450	2.049	2.035	1.957	1.984	1.989
established Li (3–-Y)	0.371	0.384	0.404	0.432	0.400	0.951	0.949	0.550	0.951	0.965	0.043	0.026*	0.011*
Ca	0.00	0.00	0.00	0.00	0.00	0.00	0.00	0.01	0.03	0.02	0.004	0.01	0.00
Na	0.03	0.04	0.03	0.02	0.00	0.00	0.00	0.04	0.03	0.01	0.004	0.01	0.01
K	1.02	1.01	1.03	1.02	0.98	0.96	0.87	0.91	0.76	0.74	0.951	0.89	0.91
ΣX	1.05	1.05	1.06	1.05	0.98	0.97	0.868	0.96	0.81	0.77	0.959	0.91	0.92
muscovite	0.0395	0.0089	0.0004	0.0350	0.1591	0.4784	0.4762	0.2164	0.5743	0.4715	0.7585	0.7597	0.7268
Fe-celadonite	0.0000	0.0000	0.0000	0.0000	0.0000	0.0000	0.0000	0.0000	0.0000	0.0000	0.2392	0.1556	0.1645
Mg-celadonite	0.0000	0.0000	0.0000	0.0000	0.0000	0.0000	0.0000	0.0000	0.0000	0.0000	0.0000	0.0586	0.0552
masutomilite	0.0621	0.0698	0.0483	0.0366	0.0170	0.0353	0.0421	0.0151	0.0046	0.0000	0.0172	0.0000	0.0000
polylithionite	0.1545	0.1593	0.1807	0.1988	0.1855	0.3744	0.3665	0.2592	0.3781	0.4766	0.0000	0.0122	0.0573
Ti-biotite	0.0529	0.0605	0.0664	0.0582	0.0199	0.0000	0.0000	0.0070	0.0000	0.0000	0.0000	0.0000	0.0000
annite	0.3746	0.3884	0.3804	0.3526	0.3419	0.1181	0.1157	0.3058	0.0518	0.0854	0.0000	0.0000	0.0000
siderophyllite	0.3186	0.3153	0.3261	0.3224	0.2832	0.0000	0.0000	0.1994	0.0000	0.0000	0.0000	0.0000	0.0000
Σ	1.0022	1.0022	1.0023	1.0037	1.0067	1.0062	1.0005	1.0029	1.0088	1.0336	1.0149	0.9861	1.0034

Cation proportions recalculated to 11 oxygen atoms, * in case of dioctahedral micas, assumed Li = 2–Y

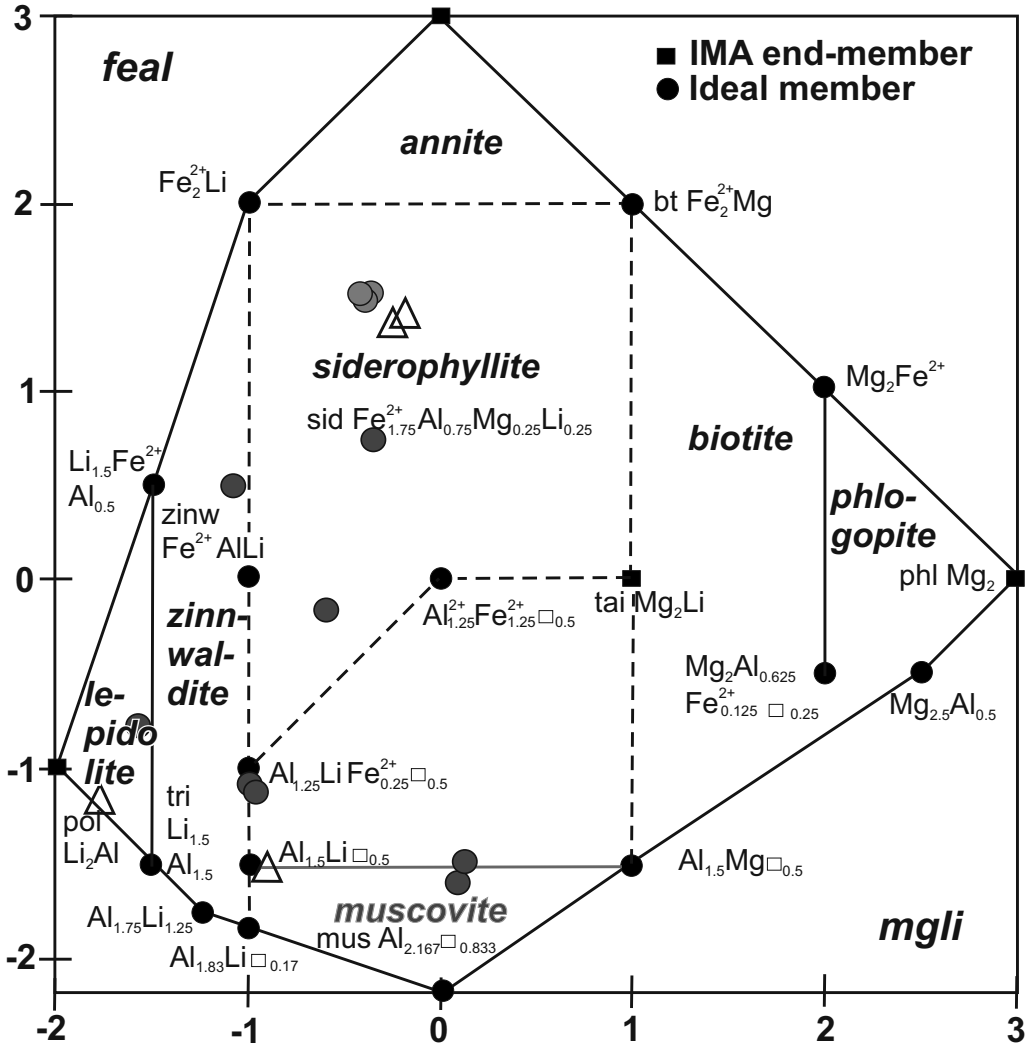

Fig. 5 Subdivision of common K-mica varieties in the mgli–feal diagram (Tischendorf et al. 2004); mgli = (Mg – Li); feal = (Fe_{tot} + Mg + Ti – ^{VI}Al).

4.2. Greisens

The greisens occur mainly as zones of alteration, concentrated along the margin of the intrusion and in the regions of intense fracturing of the BGC Pluton (Fig. 2). They reveal strong mineralogical diversity. The most frequently observed type are *dark mica (biotite–zinnwaldite)–quartz greisens*, with differing proportions of the two main minerals. The second type, the *light quartz–mica (muscovite–lepidolite) greisens*, is characterized by an elevated quartz content. The *quartz–fluorite greisens*, with violet and green fluorite mineralization, contain subordinate white micas (muscovite–lepidolite) (Tab. 1, Fig. 5). In places, they are strongly deformed, which is taken as an evidence of their genetic relation with the older dislocation zones. The last type of greisens resembles *strongly altered granites*. They display relic granitic textures, and contain remnants of magmatic minerals (such as feldspars and biotites replaced by mica aggregates) as well as high fluorite and topaz contents.

5. Granite geochemistry

The compositions of selected, representative granitic rocks are presented in Tab. 2, further data and details can be found in the preceding specific geochemical study (Machowiak and Stawikowski 2012).

The BGC granites are characterized by high SiO_2 contents (73.7–80.2 wt. %, av. 76.4 wt. %), and distinctly elevated alkalis (K_2O 3.8–6.6 wt. %, av. 4.9 wt. %, Na_2O 2.8–3.9 wt. %, 3.3 wt. %). The alumina saturation index (A/CNK = Al_2O_3/($CaO + Na_2O + K_2O$) in mol. %) is close to 1. The magnesium number (Mg# = Mg/(Mg + Fe) in mol. %) is usually low but variable (1.9–20.5, typically below 10) (Machowiak and Stawikowski 2012).

The contents of selected trace elements in the granites are presented in a spider diagram normalized to the composition of the average continental crust (Fig. 6). The BGC granites reveal strong depletions in Ba, Sr and Ti and as well as enrichments in most other trace elements, most notably Rb, Cs, Th, Ta, and HREE + Y. Their content of Eu is very low (<0.05–0.44 ppm, av. 0.17), in

Tab. 2 Selected geochemical analyses of the BGC granites (M17, M21, W78 – fine-grained granites; M1, M15, M27, K15 – medium-grained granites; M25 – coarse-grained granite).

	M17	M21	W78	M1	M15	M27	K15	M25
SiO_2	75.94	75.97	75.92	75.91	78.1	75.82	77.86	76.02
TiO_2	0.101	0.076	0.069	0.085	0.093	0.090	0.068	0.063
Al_2O_3	12.18	12.16	12.49	12.92	11.11	12.04	11.00	12.17
Fe_2O_{3t}	0.81	1.19	1.10	1.04	0.86	1.11	0.96	0.89
MnO	0.011	0.022	0.030	0.026	0.015	0.027	0.021	0.017
MgO	0.06	0.05	0.03	0.05	0.05	0.05	0.04	0.04
CaO	0.50	0.41	0.48	0.64	0.47	0.41	0.26	0.38
Na_2O	3.15	3.37	3.39	3.25	2.81	3.18	3.14	3.35
K_2O	4.99	4.62	4.61	4.99	4.74	4.91	4.45	4.70
P_2O_5	b.d.	0.01	b.d.	0.06	b.d.	b.d.	0.03	b.d.
LOI	0.91	0.71	0.74	0.91	0.92	0.91	0.79	0.95
Total	98.64	98.60	98.90	99.870	99.18	98.56	98.60	98.60
A/CNK	1.06	1.07	1.09	1.08	1.05	1.07	1.05	1.08
Mg#	12.7	7.7	5.1	8.7	10.2	8.2	7.6	8.2
T_{Zr}	790	799	793	795	782	798	785	785
AI	0.87	0.87	0.85	0.83	0.88	0.88	0.91	0.87
Sc	3.0	3.0	5.0	4.0	3.0	4.0	3.0	3.0
Be	7.0	7.0	8.0	13.0	6.0	7.0	7.0	5.0
V	b.d.	b.d.	b.d.	b.d.	b.d.	b.d.	b.d.	b.d.
Ba	80	37	21	67	81	52	25	58
Sr	19	9.0	7.0	18	15	11	10	12
Y	99.0	137	134	130	121	117	69	92
Zr	143	152	143	152	130	153	129	130
Co	38	63	39	95	47	29	47	29
Ni	b.d.	b.d.	b.d.	b.d.	b.d.	b.d.	b.d.	b.d.
Cu	b.d.	b.d.	b.d.	b.d.	b.d.	b.d.	b.d.	b.d.
Zn	40	30	60	30	30	50	30	b.d.
Ga	24	27	26	25	23	26	20	26
Ge	2.0	3.0	3.0	3.0	2.0	3.0	2.0	2.0
As	b.d.	b.d.	b.d.	b.d.	b.d.	b.d.	b.d.	11
Rb	302	422	534	394	319	398	400	385
Nb	23	48	73	38	35	53	34	40
Mo	b.d.	b.d.	b.d.	b.d.	b.d.	b.d.	b.d.	b.d.
Ag	0.6	0.7	0.8	0.5	0.6	0.6	0.7	0.6
In	b.d.	b.d.	b.d.	b.d.	9.0	b.d.	b.d.	b.d.
Sn	9.0	55.0	132	232	2.2	8.0	13.0	13.0
Sb	2.0	1.7	b.d.	1.4	10.7	1.4	b.d.	1.8
Cs	8.1	10.4	21.7	18.4	46.3	12.5	16.0	13.1
La	56.8	50.3	54.7	46.9	46.3	59.7	34.8	34.7
Ce	128	109	119	101	99.3	130	74.0	78.5
Pr	14.4	13.6	12.7	12.4	12.1	15.4	7.72	9.14
Nd	50.1	46.9	43.0	44.2	43.8	51.4	25.7	31.0
Sm	12.2	12.5	10.9	11.9	11.0	12.4	6.1	8.1
Eu	0.34	0.12	0.06	0.20	0.23	0.22	0.11	0.18
Gd	11.4	12.7	11.8	12.0	11.4	11.7	6.4	8.1
Tb	2.3	2.7	2.6	2.5	2.4	2.4	1.4	1.8
Dy	14.8	19.4	18.4	17.1	16.2	17.0	9.4	13.0
Ho	3.1	4.1	4.1	3.7	3.6	3.6	2.1	2.8
Er	9.9	13.4	13.8	12.1	11.2	11.6	6.7	8.8
Tm	1.69	2.37	2.51	2.05	1.89	1.97	1.18	1.48
Yb	11.7	17.2	17.6	14.2	13.1	14.0	8.1	10.6
Lu	1.85	2.76	2.8	2.25	2.09	2.22	1.27	1.77
Hf	6.6	9.3	9.3	6.7	6.7	8.5	7.0	7.7
Ta	2.6	5.6	9.4	4.4	3.6	7.3	4.2	4.9
W	360	615	460	745	517	331	414	355
Tl	1.5	2.3	2.9	2.2	1.7	2.3	1.9	2.3
Pb	40	39	28	34	39	35	33	27
Bi	b.d.	b.d.	3.5	2.7	1.6	2.6	b.d.	4.7
Th	35.3	56.8	45.8	38.3	34.6	43.9	26.5	40.5
U	6.7	7.8	9.6	15.4	4.9	3.7	6.1	4.8
ΣREE	318.6	307.1	313.9	282.5	274.6	333.6	184.9	209.9
Eu/Eu*	0.09	0.03	0.02	0.05	0.06	0.06	0.05	0.07

A/CNK – alumina saturation index, $Al_2O_3/(CaO + Na_2O + K_2O)$ in mol. %
Mg# – Mg/(Mg + Fe) in mol. %
T_{Zr} – zircon saturation temperatures in ºC
AI – agpaitic index $(Na_2O + K_2O)/Al_2O_3$ in mol. %
ΣREE – total contents of rare earth elements
Eu/Eu* – $Eu/\sqrt{(Sm \times Gd)}$

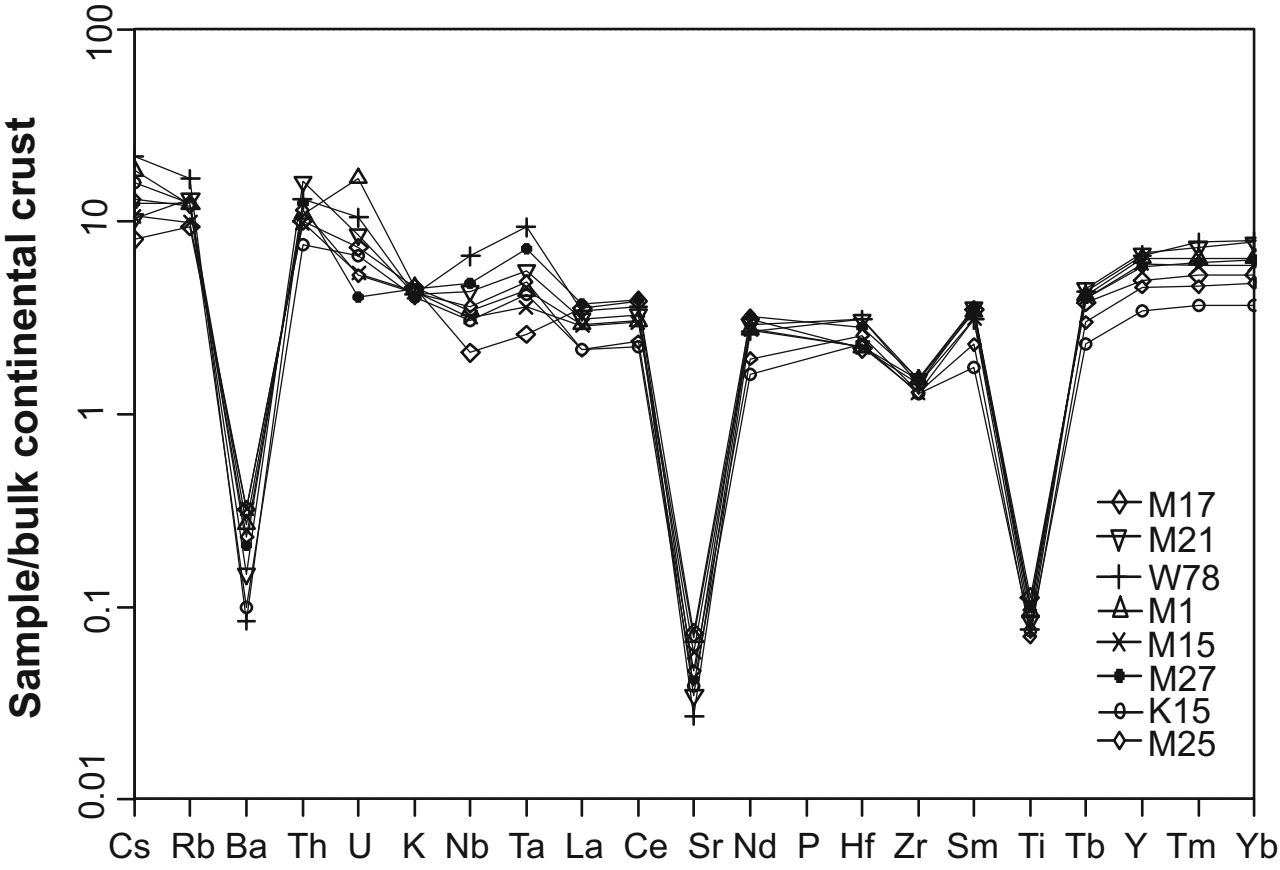

Fig. 6 Spider diagram of the Baga-Gazryn Chuluu granites normalized to bulk continental crust (Taylor and McLennan 1995; samples: M17, M21, W78 – fine-grained granites; M1, M15, M27, K15 – medium-grained granites; M25 – coarse-grained granite).

contrast to the remaining REE, sum of which is 131–428 ppm (av. 255). The chondrite-normalized patterns (Fig. 7) are fairly flat (LREE/HREE (La_N/Yb_N) = 1.82 and 6.48 (av. 3.88)) and characterized by deep negative Eu anomalies (Eu/Eu* ratio, defined as $Eu/\sqrt{(Sm \times Gd)}$), being less than 0.02–0.16 (av. 0.057)).

In majority of the samples, the "lanthanide tetrad effect" has been observed (Machowiak and Stawikowski 2012), typical of highly evolved granites, mainly those characterized by significant contents of volatiles at the final stage of crystallization (e.g. Masuda et al. 1987; Irber 1999). The distinct Eu anomaly as well as the trends

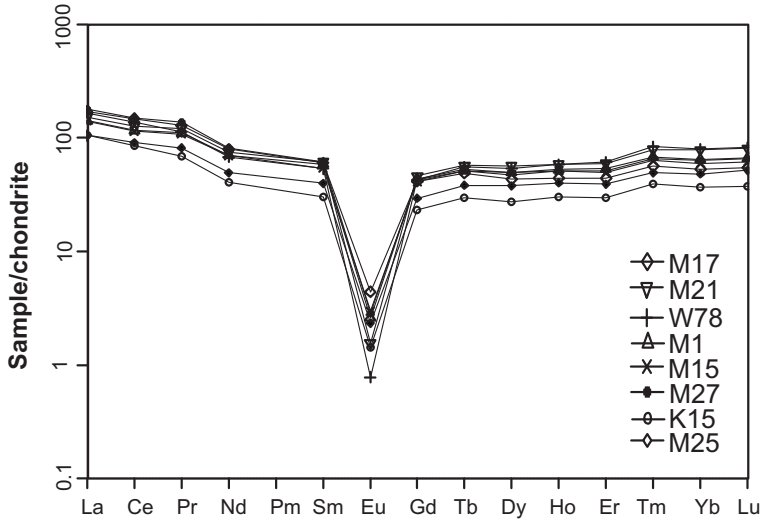

Fig. 7 Chondrite-normalized REE plots of the BGC granites (normalized to values given in Nakamura 1974; symbols as in Fig. 6).

Tab. 3 Tabulated results of Ar–Ar dating

coarse-grained granite (sample M25) J = 0.003650 ± 0.000035

T°C	$^{40}Ar\ cm^3$ (STP)	$^{40}Ar/^{39}Ar$	±1σ	$^{38}Ar/^{39}Ar$	±1σ	$^{37}Ar/^{39}Ar$	±1σ	$^{36}Ar/^{39}Ar$	±1σ	Ca/K	$\sum^{39}Ar$ (%)	Age	±1σ
500	25.2×10^{-9}	34.879	0.027	0.02565	0.00182	0.01902	0.00371	0.05458	0.00176	0.068	1.1	119.4	3.4
600	256.0×10^{-9}	35.957	0.011	0.01973	0.00015	0.00307	0.00035	0.02118	0.00015	0.011	12.3	185.7	1.7
700	999.1×10^{-9}	33.511	0.004	0.01624	0.00007	0.00227	0.00007	0.00380	0.00003	0.008	59.1	201.6	1.8
750	334.1×10^{-9}	32.632	0.008	0.01538	0.00016	0.00072	0.00031	0.00126	0.00018	0.003	75.1	200.8	1.8
800	145.8×10^{-9}	32.688	0.008	0.01635	0.00002	0.00239	0.00026	0.00308	0.00027	0.009	82.1	198.0	1.9
900	274.9×10^{-9}	32.410	0.007	0.01585	0.00015	0.00330	0.00032	0.00207	0.00019	0.012	95.4	198.1	1.8
1060	89.3×10^{-9}	35.465	0.017	0.02101	0.00060	0.00808	0.00075	0.01013	0.00105	0.029	99.4	202.1	2.6
1130	15.8×10^{-9}	39.077	0.127	0.02178	0.00405	0.00191	0.00447	0.02029	0.00369	0.007	100.0	205.7	6.7

medium-grained granite (sample K15) J = 0.003760 ± 0.000037

T°C	$^{40}Ar\ cm^3$ (STP)	$^{40}Ar/^{39}Ar$	±1σ	$^{38}Ar/^{39}Ar$	±1σ	$^{37}Ar/^{39}Ar$	±1σ	$^{36}Ar/^{39}Ar$	±1σ	Ca/K	$\sum^{39}Ar$ (%)	Age	±1σ
500	21.8×10^{-9}	47.285	0.079	0.02771	0.00279	0.02461	0.00508	0.07433	0.00196	0.089	0.7	164.1	3.9
600	129.0×10^{-9}	41.636	0.012	0.02119	0.00039	0.00607	0.00044	0.03189	0.00023	0.022	5.6	206.3	2.0
700	451.6×10^{-9}	34.067	0.007	0.01548	0.00009	0.00506	0.00027	0.00284	0.00011	0.018	26.4	212.4	2.0
775	429.5×10^{-9}	33.681	0.005	0.01523	0.00003	0.00503	0.00006	0.00236	0.00006	0.018	46.3	210.9	2.0
875	132.5×10^{-9}	34.772	0.011	0.01652	0.00036	0.00989	0.00112	0.00495	0.00037	0.036	52.3	212.9	2.1
960	418.3×10^{-9}	33.898	0.006	0.01551	0.00013	0.00597	0.00023	0.00300	0.00010	0.021	71.7	211.1	2.0
1000	477.3×10^{-9}	33.840	0.003	0.01526	0.00009	0.00510	0.00017	0.00235	0.00014	0.018	93.8	211.9	2.0
1025	103.1×10^{-9}	36.855	0.015	0.01787	0.00038	0.00887	0.00037	0.01200	0.00055	0.032	98.2	212.9	2.2
1130	43.1×10^{-9}	36.670	0.047	0.02101	0.00086	0.00697	0.00214	0.01329	0.00053	0.025	100.0	209.5	2.2

fine-grained granite (sample W78) J = 0.003130 ± 0.000026

T°C	$^{40}Ar\ cm^3$ (STP)	$^{40}Ar/^{39}Ar$	±1σ	$^{38}Ar/^{39}Ar$	±1σ	$^{37}Ar/^{39}Ar$	±1σ	$^{36}Ar/^{39}Ar$	±1σ	Ca/K	$\sum^{39}Ar$ (%)	Age	±1σ
500	28.7×10^{-9}	56.828	0.177	0.02774	0.00147	0.03673	0.00363	0.07484	0.00249	0.132	15.6	224.4	22.5
600	176.3×10^{-9}	48.373	0.025	0.02028	0.00031	0.01347	0.00040	0.02893	0.00033	0.048	31.5	257.9	17.1
700	471.8×10^{-9}	41.585	0.008	0.01557	0.00009	0.01450	0.00015	0.00511	0.00008	0.052	56.6	262.4	12.3
775	647.5×10^{-9}	40.415	0.007	0.01511	0.00009	0.00798	0.00017	0.00278	0.00004	0.029	69.8	263.7	17.8
825	289.0×10^{-9}	40.678	0.014	0.01580	0.00014	0.00872	0.00040	0.00457	0.00016	0.031	82.4	249.6	19.1
900	659.7×10^{-9}	40.699	0.005	0.01561	0.00006	0.00426	0.00003	0.00445	0.00007	0.015	100.0	333.4	15.1
950	610.2×10^{-9}	40.189	0.008	0.01535	0.00006	0.00688	0.00018	0.00298	0.00010	0.025	15.6	224.4	22.5
975	841.5×10^{-9}	39.945	0.006	0.01499	0.00005	0.01257	0.00009	0.00221	0.00005	0.045	31.5	257.9	17.1
1000	533.6×10^{-9}	39.824	0.006	0.01508	0.00009	0.00993	0.00011	0.00208	0.00006	0.036	56.6	262.4	12.3
1025	173.7×10^{-9}	40.448	0.013	0.01555	0.00046	0.00959	0.00042	0.00441	0.00047	0.035	69.8	263.7	17.8
1075	110.5×10^{-9}	40.785	0.025	0.01700	0.00057	0.00744	0.00129	0.00678	0.00059	0.027	82.4	249.6	19.1
1130	19.2×10^{-9}	51.241	0.338	0.03127	0.00529	0.01766	0.01083	0.04546	0.00396	0.064	100.0	333.4	15.1

STP – Standard Temperature and Pressure

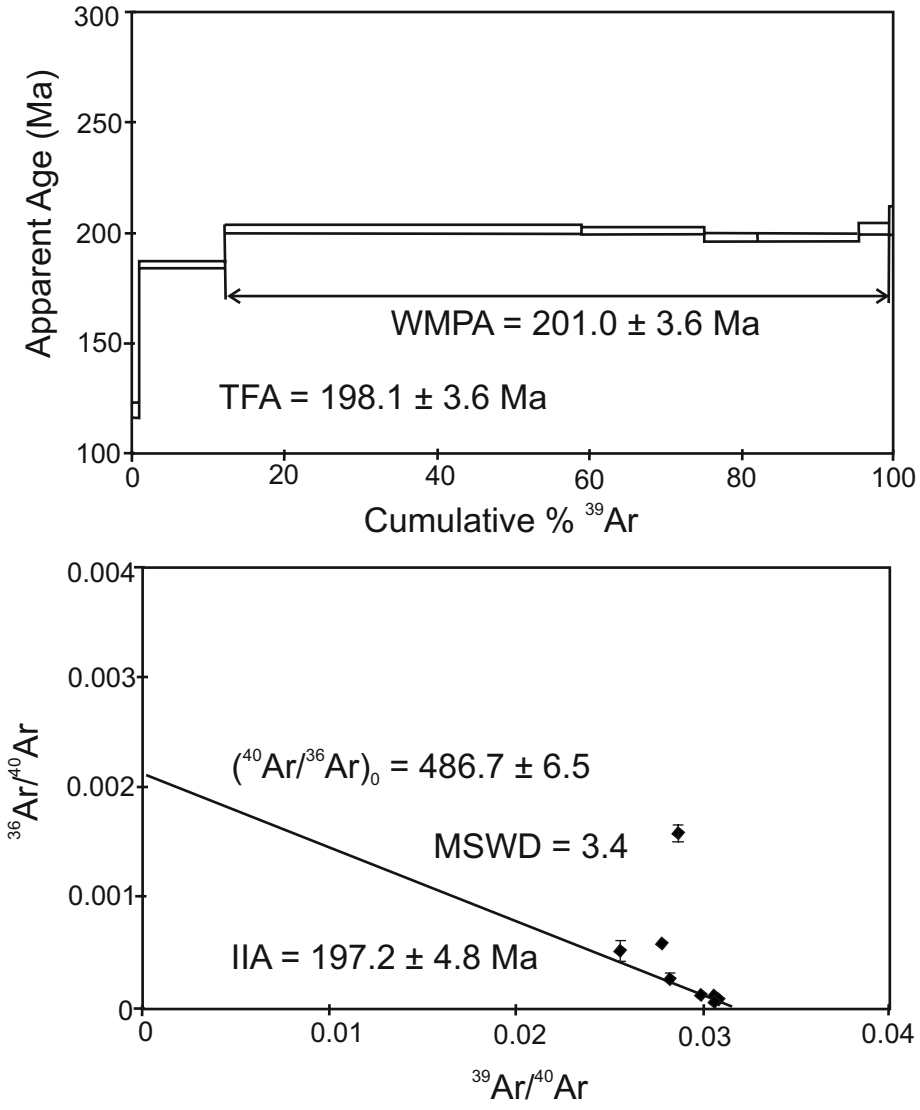

Fig. 8 Plateau plot and inverse isochron diagram of coarse-grained granite M25. WMPA – weighted mean plateau age, TFA – total fusion age, MSWD – mean squared weighted deviation, IIA – inverse isochron age.

in the REE diagram (Fig. 7) are characteristic of strongly fractionated rocks that originated from crustal material. The elevated HREE contents suggest an absence of garnet in the residue during anatexis (e.g. Rollinson 1993). The studied rocks display also high Rb/Sr ratios (8–88 ppm, av. 45.5). The postmagmatic processes resulted in an increase of W (455–1370 ppm, av. 730), and, in places, Sn (<1–232 ppm, av. 17.8).

The crystallization temperatures have been calculated for the BGC granitic rocks, using zircon saturation ther-

Tab. 4 Summary table of $^{40}Ar/^{39}Ar$ results for studied biotite separates

Sample	IIA (Ma) ±2σ*	TFA (Ma)† ±2σ	WMPA (Ma)‡ ±2σ	Ca/K§	Comments
M25 biotite	197.2 ± 4.8	198.1 ± 3.6	201.0 ± 3.6	0.003–0.068	Five steps plateau
K15 biotite	210.0 ± 4.6	211.1 ± 4.0	211.9 ± 4.0	0.018–0.089	Six steps plateau
W78 biotite	208.5 ± 3.6	209.8 ± 3.2	209.4 ± 3.2	0.015–0.132	Seven steps plateau

* – Inverse isochron ages, σ – estimated uncertainties (2 sigma)
† – Total fusion ages
‡ – Weighted mean plateau ages
§ – Apparent Ca/K ratios

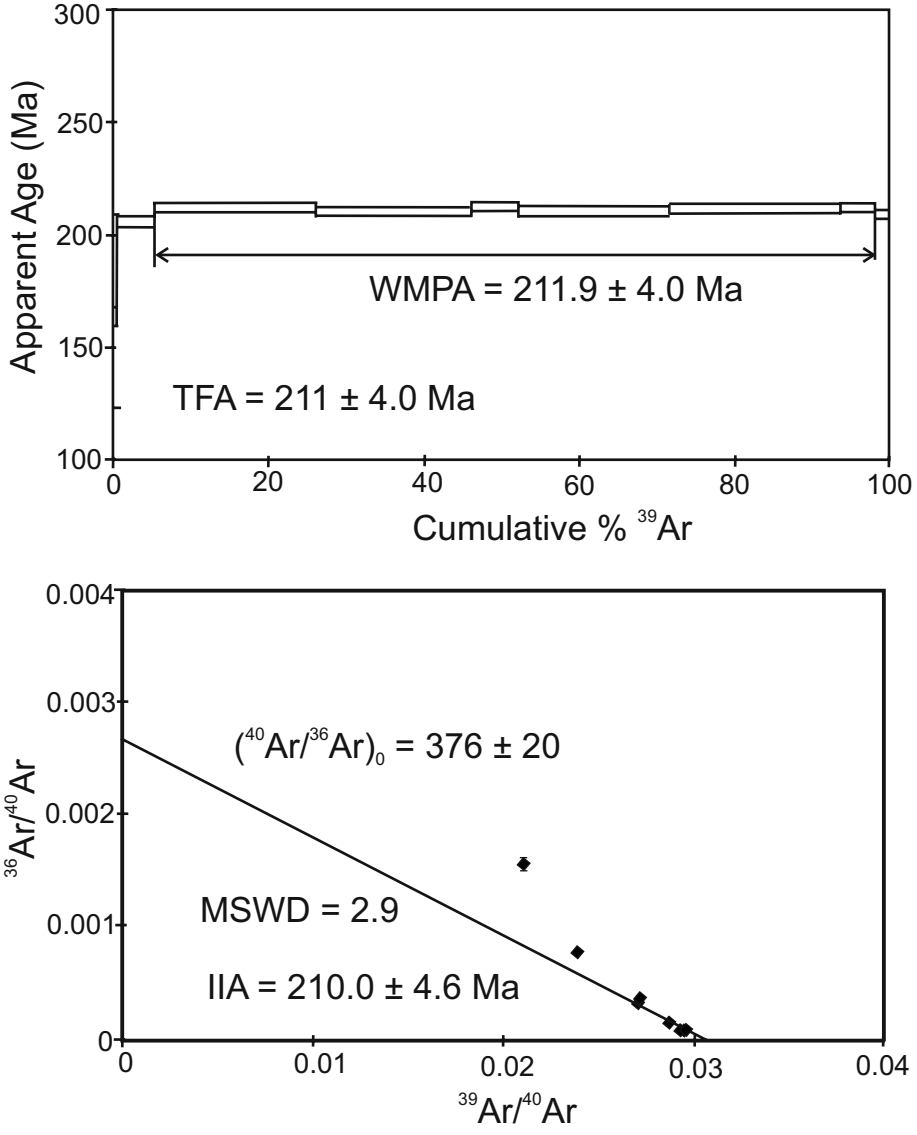

Fig. 9 Plateau plot and inverse isochron diagram of medium-grained granite K15. Abbreviations as on Fig. 8.

mometry of Watson and Harrison (1983). For the most granite samples, the obtained values are relatively high, *c.* 800 ºC (Machowiak and Stawikowski 2012).

6. Results of ^{40}Ar–^{39}Ar dating

Due to the absence of large enough zircon grains to be analyzed by SHRIMP (>50 μm), Ar–Ar dating method on biotite concentrates has been applied in order to constrain the emplacement/cooling ages of the individual facies within the BGC Pluton. Taking into account that greisenization may potentially disturb $^{40}Ar/^{39}Ar$ isotope ratios in micas (e.g. Smith et al. 2005), dating samples have been collected far from the greisenization zones. The field and microscopic observations further helped to select the samples with fresh and homogenous biotite.

The biotite concentrates were prepared from the most representative samples of three main granite varieties of the Baga-Gazryn Chuluu Pluton (Fig. 2): (1) fine-grained equigranular granite W78 (Fig. 3a) from the western margin (46° 12' 38.9" N, 105° 58' 19.3" E). (2) medium-grained porphyritic granite K15 (Fig. 3b) coming from the NE part (46° 13' 38.4" N, 106° 05' 26.6" E), and (3) coarse-grained porphyritic granite M25 (Fig. 3c) collected in the central part of the Pluton (46° 12' 55.9" N, 106° 00' 48.1" E). The results of ^{40}Ar–^{39}Ar radiometric dating (Tab. 3) are documented by the plateau and inverse isochron diagrams (Figs 8–10) and also presented in a synthetic table (Tab. 4).

The three analysed biotite concentrates from the BGC granites yielded weighted mean plateau ages of 209.4 ± 3.2 Ma (2σ, fine-grained granite W78), 211.9 ± 4.0 Ma (medium-grained granite K15), and 201.0 ± 3.6 Ma (coarse-grained granite M25). The $^{36}Ar/^{40}Ar$ isotope

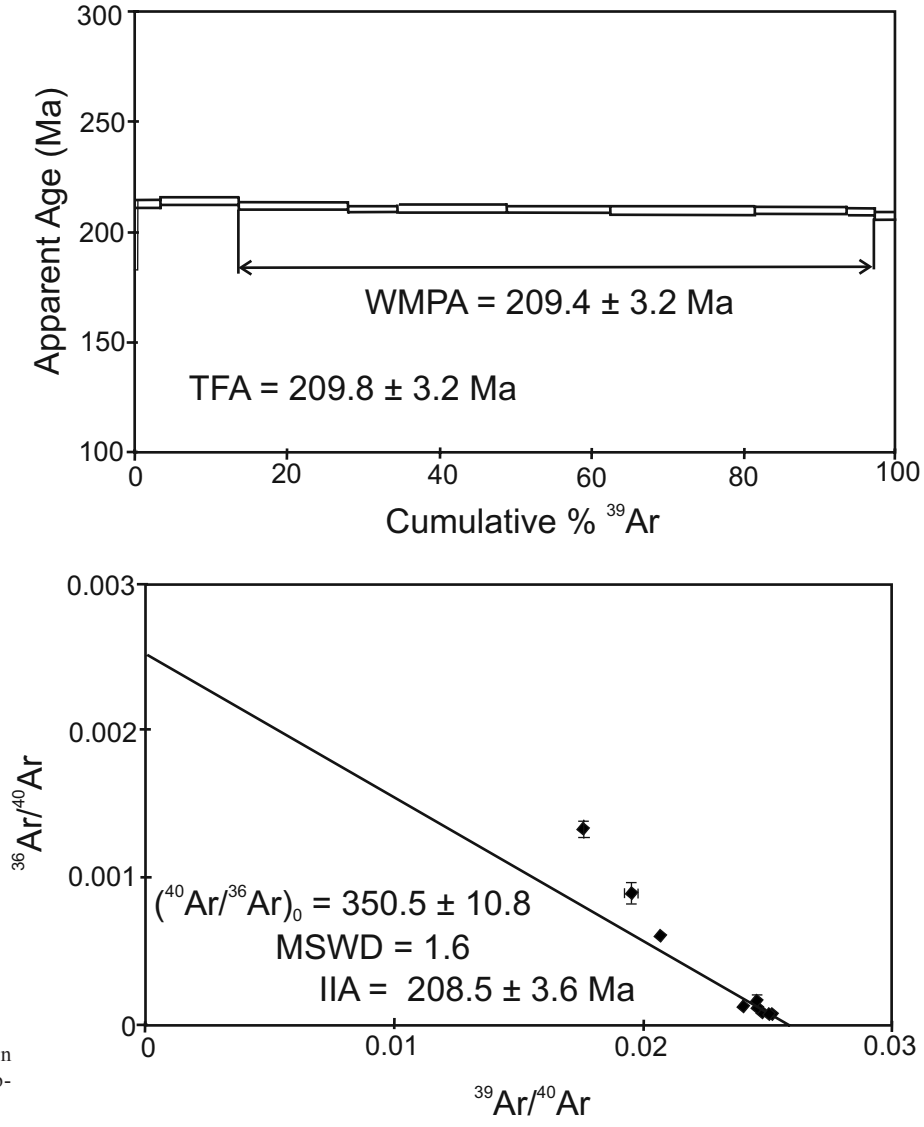

Fig. 10 Plateau plot and inverse isochron diagram of fine-grained granite W78. Abbreviations as on Fig. 8.

initial ratios seem to be overestimated, as the inverse isochron diagrams are partly non-linear.

7. Discussion and conclusions

The Late Triassic cooling ages from the Baga-Gazryn Chuluu Pluton in principle confirm the previous K–Ar dating (whole rock, biotite and K-feldspar) and the interpretation of regional geology (e.g. Kovalenko et al. 1971a, b; Tomurtogoo et al. 1998–2002). Surprisingly, the youngest age was determined for the coarse-grained granite from the inner part of the intrusion. This disagrees with Kovalenko et al. (1971a) who assumed that the coarse-grained variety was older than the finer grained granite types of the BGC. However, radiogenic Ar could have been diffusively lost from biotite due to thermodynamic disequilibrium, initiated e.g. by temperature fluctuations and/or greisenization in the BGC granites. Therefore, the obtained ages should be treated as minimal constraints and caution should be exercised in interpretation of the obtained age differences for the three textural varieties of the BGC granites.

The advanced greisenization of the granites is testified, *inter alia*, by their modal composition, in places enriched in lithium micas and other minerals connected with such processes. Also based on the field observations – common occurrences of mutual interfingering between at least two types of the granite – it can be assumed that the time intervals between the successive magmatic pulses in the BGC Pluton were short enough to sustain plastic behavior of the contacting varieties of granites.

Relics of the rocks which are considered as transitional to volcanic facies were found in the envelope near the NE border of the Pluton (Fig. 11). These felsites characterized by large K-feldspar phenocrysts and very-

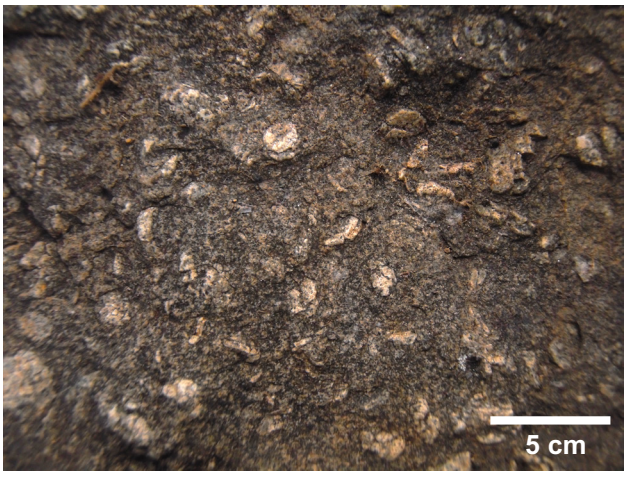

Fig. 9 Photograph of a (?subvolcanic) rock transitional between granite and rhyolite.

fine-grained groundmass are taken as an evidence that the BGC Pluton was a shallow, possibly subvolcanic intrusion with volcanic cover. The presence of weakly developed, narrow contact aureole around the Pluton also supports the relatively shallow emplacement level of the BGC intrusion.

The trachyandesites occurring near the BGC Pluton are most probably older than the granite intrusion, although no cross-cutting relationships were observed in the field. However, the trachyandesites are structurally conformable with the sedimentary cover of the Pluton.

The BGC granitic body is situated adjacent to regional-scale dislocation zone connected with the Mid-Mongolian Tectonic Line (Tomurtogoo 1997), a large tectonic lineament, which formed as a result of the Mongol–Okhotsk Ocean closure (Donskaya et al. 2012). While the collision in the eastern part of this oceanic domain took place in Middle (Tomurtogoo et al. 2005) or Late Jurassic (Zonenshain et al. 1990) or even in Early Cretaceous (Cogne et al. 2005), it probably proceeded diachronically, in the "scissor-like fashion" from west to east (e.g. Bat-Ulzii et al. 2004; Machowiak and Stawikowski 2012). This would explain the younger age of the closure recorded in the eastern part of the tectonic suture and the older age in its western part, where the presented plutonic body is located. However, the BGC granites did not form during the subduction and collision stages, which in the studied area took place in the latest Paleozoic (e.g. Bussien et al. 2011) but rather due to post-convergent activity of the suture zone area in the extensional regime.

The geochemical signature of the BGC Pluton granites as well as the zircon saturation temperatures may indicate a shallow, crustal source subjected to melting at relatively high temperatures. The granites crystallized from completely molten magma, which is evidenced by an absence of restitic enclaves. The feasible model would be partial melting of continental crust due to its basal heating by mantle magmas rising into the shallow lithosphere (Machowiak and Stawikowski 2012). The contribution of mantle magma in the melt seems to be possible, although at the current stage of study, without isotopic data, difficult to prove. However, it seems to be more likely that the role of mantle magmas was limited only to be a heat generator, which initialized the crustal anatexis.

Indeed, as the nearby Adaatsag Ophiolite (*c.* 30 km to NE from the Baga-Gazryn Chuluu area) was dated as Carboniferous (Tomurtogoo et al. 2005), one should assume, that the closure of Mongol–Okhotsk Ocean in this part of the suture commenced not earlier than in the Latest Paleozoic. This is additionally documented by the Late Paleozoic age of granitoids in this region (Oyungerel and Ishihara 2005), which are most likely connected with subduction/collisional setting. On the other hand, the younger, anorogenic granites of Mesozoic age (Oyungerel and Ishihara 2005), including the BGC Pluton granites, intruded already in the extensional regime (Machowiak and Stawikowski 2012). The current ^{40}Ar–^{39}Ar study of the Baga-Gazryn Chuluu Pluton confirms the Mesozoic age of the A- type granites occurring in this area, and is the step to elucidate the evolution of magmatism near the Mid-Mongolian Tectonic Line. It indicates the necessity of follow-up radiometric investigations on granitoid rocks of similar type, located in the vicinity of this important structural zone.

Acknowledgements. The research was funded by Polish Ministry of Science and High Education grant no. N N307 225835. The authors address sincere thanks to Dr. Dash Bat-Ulzii from the School of Geology, Petroleum Engineering, Mongolian University Science and Technology, for delivery of helpful cartographic materials concerning the study area and for valuable instructions during the organization of fieldwork. They thank also Mr. Sanjsuren Boldbaatar, the General Director of Jules Vernes Mongolia Co., for his great help in organization of the expeditions, logistic facilities, transfer of the samples to Poland and great kindness. The authors are very grateful to Prof. Mao Jingwen, Prof. Ochir Gerel and Dr. Pavel Hanžl, for their constructive reviews and to Handling Editor, Prof. Miroslav Štemprok and Editor-in-Chief, Assoc. Prof. Vojtech Janoušek for their thorough and adequate comments, which significantly improved the final version of the paper.

References

Badarch G, Cunningham WD, Windley BF (2002) A new terrane subdivision for Mongolia: implications for the

Phanerozoic crustal growth of Central Asia. J Asian Earth Sci 21: 87–110

Bat-Ulzii D, Gantumur H, Gandush B (2004) Late Mesozoic volcanic activity in Mongolia: implications for post-collisional magmatic evidence resulting from the closure of Mongol–Okhotsk oceanic basin. In: Khanchuk AI, Gonevchuk GA, Mitrokhin AN, Simanenko LF, Cook NJ, Seltmann R (eds) Proceedings of the IAGOD Conference, Dalnauka, Vladivostok, pp 77–79

Bussien D, Gombojav N, Winkler W, von Quadt A (2011) The Mongol–Okhotsk Belt in Mongolia – an appraisal of the geodynamic development by the study of sandstone provenance and detrital zircons. Tectonophysics 510: 132–150

Cogne JP, Kravchinsky VA, Halim N, Hankard F (2005) Late Jurassic–Early Cretaceous closure of the Mongol–Okhotsk Ocean demonstrated by new Mesozoic palaeomagnetic results from the Trans-Baikal area (SE Siberia). Geophys J Int 163: 813–832

Donskaya TV, Gladkochub DP, Mazukabzov AM, De Waele B, Presnyakov SL (2012) The Late Triassic Kataev volcanoplutonic association in western Transbaikalia, a fragment of the active continental margin of the Mongol–Okhotsk Ocean. Russ Geol Geophys 53: 22–36

Irber W (1999) The lanthanide tetrad effect and its correlation with K/Rb, Eu/Eu*, Sr/Eu, Y/Ho, and Zr/Hf of evolving peraluminous granite suites. Geochim Cosmochim Acta 63: 489–508

Jahn B-M (2004) The Central Asian Orogenic Belt and growth of the continental crust in the Phanerozoic. In: Malpas J, Fletcher CJN, Ali JR, Aitchison JC (eds) Aspects of the Tectonic evolution of China. Geological Society London Special Publications 226: 73–100

Jahn B-M, Litvinovsky BA, Zanvilevich AN, Reichow M (2009) Peralkaline granitoid magmatism in the Mongolian–Transbaikalian Belt: evolution, petrogenesis and tectonic significance. Lithos 30: 1–19

Kovalenko VI, Kuzmin MI, Zonenshain LP, Nagibna MS, Pavlenko AS, Vladikin NB, Tseden TS, Gundsambu TS, Goreglyad AV (1971a) The Baga Gazryn Massif of the 'Sharakhadinskii' type granites and the accompanying tin deposits. In: Zaitsev NS, Tauson LV, Luwsan-Danzan B, Luchitsky IV, Menner VV, Pavlova TG, Peive AV, Timofeev PP, Tomurtogoo O, Yanshin AL (eds) Rare metal granitoids of Mongolia (petrology, distribution of rare elements and genesis). Transactions 5 of Joint Soviet–Mongolian scientific research geological expedition. Nauka, Moscow, pp 61–69 (in Russian)

Kovalenko VI, Kuzmin MI, Zonenshain LP, Nagibna MS, Pavlenko AS, Vladikin NB, Tseden TS, Gundsambu TS, Goreglyad AV (1971b) General geological characteristics of the Mesozoic "rare metal" granitoids of the Mongolian People's Republic. In: Zaitsev NS, Tauson LV, Luwsan-Danzan B, Luchitsky IV, Menner VV, Pavlova TG, Peive AV, Timofeev PP, Tomurtogoo O, Yanshin AL (eds) Rare metal granitoids of Mongolia (petrology, distribution of rare elements and genesis). Transactions 5 of Joint Soviet–Mongolian scientific research geological expedition. Nauka, Moscow, pp 17–37 (in Russian)

Machowiak K, Stawikowski W (2012) The Baga-Gazriin Chuluu A-type granites of Central Mongolia compared with other igneous bodies nearby: a geochemical approach. Geol Q 56: 455–472

Masuda A, Kawakami O, Dohmoto Y, Takenaka T (1987) Lanthanide tetrad effects in nature: two mutually opposite types W and M. Geochem J 21: 119–124

Nakamura N (1974) Determination of REE, Ba, Fe, Mg, Na and K in carbonaceous and ordinary chondrites. Geochim Cosmochim Acta 38: 757–773

Oyungerel S, Ishihara S (2005) Paleozoic and Mesozoic granitic rocks in the Hotont area, central Mongolia. Bull Geol Surv Jap 56: 245–258

Reed SJB (1993) Electron Microprobe Analysis and Scanning Electron Microscopy in Geology. Cambridge University Press, New York, pp 1–215

Rieder M, Cavazzini G, D'yakonov J, Kamenetskii F, Gottardi G, Guggenheim S, Koval P, Müller G, Neiva AMR, Radoslovich E, Robert JL, Sassi FP, Takeda H, Weiss Z, Wones DR (1998) Nomenclature of the micas. Canad Mineral 36: 1–8

Rollinson H (1993) Using Geochemical Data: Evaluation, Presentation, Interpretation. Longman, London, pp 1–352

Smith SR, Kelley CSP, Tindle CAG, Breaks CFW (2005) Compositional controls on $^{40}Ar/^{39}Ar$ ages of zoned mica from a rare-element pegmatite. Contrib Mineral Petrol 149: 613–626

Tajčmanová L, Connolly JAD, Cesare B (2009) A thermodynamic model for titanium and ferric iron solution in biotite. J Metamorph Geol 27: 153–165

Taylor SR, McLennan SM (1995) The geochemical evolution of the continental crust. Rev Geophys 33: 241–265

Tischendorf G, Rieder M, Förster HJ, Gottesmann B, Guidotti ChV (2004) A new graphical presentation and subdivision of potassium micas. Mineral Mag 68: 649–667

Tomurtogoo O (1997) A new tectonic scheme of the Paleozoides in Mongolia. MG 3: 19–22

Tomurtogoo O, Byamba J, Badarch G, Minjin Ch, Orolmaa D, Khosbayar P, Chuluun D, Makhbadar T, Bat-Ireedui T (1998–2002) Geological Map of Mongolia, scale: 1: 1000 000. Mongolian Academy of Sciences, Institute of Geology and Mineral Resources, Ulaanbaatar

Tomurtogoo O, Windley BF, Kröner A, Badarch G, Liu DY (2005) Zircon age and occurrence of the Adaatsag ophiolite and Muron shear zone, central Mongolia: constraints on the evolution of the Mongol–Okhotsk

Ocean, suture and orogen. J Geol Soc, London 162: 125–134

White RW, Powell R, Holland TJB (2007) Progress relating to calculation of partial melting equilibria for metapelites. J Metamorph Geol 25: 511–527

Wilhem C, Windley BF, Stampfli GM (2012) The Altaids of central Asia: a tectonic and evolutionary innovative review. Earth Sci Rev 113: 303–341

Windley BF, Alexeiev D, Xiao W, Kröner A, Badarch G (2007) Tectonic models for accretion of the Central Asian Orogenic Belt. J Geol Soc, London 164: 31–47

Watson EB, Harrison M (1983) Zircon saturation revisited: temperature and composition effects in a variety of crustal magma types. Earth Planet Sci Lett 64: 295–304

Zonenshain LP, Kuzmin MI, Natapov LM (1990) Geology of the USSR: A Plate Tectonic Synthesis. American Geophysical Union, Geodynamics Series 21: 1–242